Thermal and mechanical properties of hardened cement paste reinforced with Posidonia-Oceanica natural fibers

Ons Hamdaoui, Oualid Limam, Laurent Ibos, Atef Mazioud

Thermal and mechanical properties of hardened cement paste reinforced with *Posidonia-Oceanica* natural fibers

Ons HAMDAOUI[1], Oualid LIMAM[2], Laurent IBOS[1], Atef MAZIOUD[1]

[1] University of Paris Est Créteil, CERTES, OSU Efluve, 61 av. du Général de Gaulle, 94010 Créteil Cedex, France

[2] University of Tunis El Manar, Ecole Nationale d'Ingénieurs de Tunis, Laboratoire de Génie Civil, BP 37, 1002 Tunis, Tunisia

Abstract

This paper focuses on thermal and mechanical properties of a hardened cement paste reinforced with *Posidonia-Oceanica* fibers. Fibers volume fractions are varied from 0% to 20%. Thermophysical and mechanical properties are measured. Simplified models are developed to predict thermal conductivity, tensile and compressive stresses and fracture toughness variation as a function of fibers volume fraction and geometrical characteristics of samples. Results showed that the addition of *Posidonia-Oceanica* fibers improved the material insulating properties. In fact, a decrease of about 22% (from 0.0718 $W.m^{-1}.K^{-1}$ to 0.559 $W.m^{-1}.K^{-1}$) of thermal conductivity was found with adding 20% of fibers compared to control cement paste.

Concerning mechanical properties, flexural and compressive strengths increased for fiber volume fractions in the range of 5 to 10% and then decreased for higher fiber volume fractions. It was shown through a simplified model and MEB observations that agglomeration of fibers for high volume fraction is behind this phenomenon. Moreover, a noticeable increase of toughness was observed with increasing fibers amount: for instance, an increase of about

65% (from 0.245 MPa.m$^{1/2}$ to 0.404 MPa.m$^{1/2}$) was observed with the introduction of 20% of fibers in the composite. Simplified analytical models are also developed to predict thermal conductivity, tensile and compressive strengths and fracture toughness. These models are validated with experimental data.

Key words: *natural fibers, composite, experimental measurement, models, thermal properties, mechanical properties*.

Nomenclature

- b: width of the mechanical test sample, mm
- w: depth of the mechanical test sample, mm
- L: span of the mechanical test sample, mm
- A: compressive test sample are, mm^2
- a: notch length, mm
- $\boldsymbol{\beta}$: ratio between a and w
- F_f: load required for failure in flexural test, kN
- F_c: load required for failure in compressive test, kN
- P_f : load required for failure in flexural test for pre-notched sample, kN
- k: thermal conductivity, W.m^{-1}.K^{-1}
- k_H: homogenized composite thermal conductivity, W.m^{-1}.K^{-1}
- k_m: matrix thermal conductivity, W.m^{-1}.K^{-1}

- k_f: fibers thermal conductivity, $W.m^{-1}.K^{-1}$
- k_{h1}: thermal conductivity in the volume V_2, $W.m^{-1}.K^{-1}$
- k_{h2}: thermal conductivity in the volume V_3, en $W.m^{-1}.K^{-1}$
- k_{inf}: lower thermal conductivity of the first order model, $W.m^{-1}.K^{-1}$
- k_{sup}: upper thermal conductivity of the first order model, en $W.m^{-1}.K^{-1}$
- α: thermal diffusivity, $m^2.s^{-1}$
- ρ: density, en $kg.m^{-3}$
- ρ_H: homogenized composite density, $kg.m^{-3}$
- ρ_f: fibers density, $kg.m^{-3}$
- ρ_m: matrix density, en $kg.m^{-3}$
- φ: fibers volume fraction, %
- φ_m: matrix volume fraction, %
- φ_{p1}: 'parallel' fibers volume fraction relatively to heat flux in the volume V_1, %
- φ'_{p1}: 'parallel' fibers volume fraction relatively to heat flux in the volume V_2, %
- φ_{s1}: 'series' fibers volume fraction relatively to heat flux in the volume V_2, %
- d: fibers effective diameter, mm
- d_0: fibers mean diameter, mm
- d_0': fibers equivalent diameter, mm
- l: mean length of fibers, mm

- D_1: Horizontal distance between fibers, mm
- D_2: Vertical distance between fibers, mm
- S: RVE area of dimensions $(d + D_2)^2$, mm^2
- ε: ratio between D_1 and l
- γ: ratio between D_1 and D_2
- δ: ratio between l and d_0
- $\sigma_{traction}$: tensile strength obtained by flexural test, MPa
- $\sigma_{traction,\ c}$: composite tensile strength obtained by flexural test, MPa
- $\sigma_{traction,\ T}$: direct composite tensile strength, MPa
- $\sigma_{compression,\ c}$: compressive strength, MPa
- $\sigma_{compression,\ c}$: composite compressive strength, MPa
- $\sigma_{traction,\ m}$: matrix tensile strength obtained by flexural test, MPa
- τ: interface shear strength, MPa
- K_c: fracture toughness, $MPa.m^{1/2}$
- G_c: composite fracture energy, MPa.m
- G_m: matrix fracture energy, MPa.m
- G': fracture energy of the volume containing the fiber and the matrix, MPa.m
- E_c: composite Young's modulus, MPa
- E_m: matrix Young's modulus, MPa

- E_f: fibers Young's modulus, MPa

1. Introduction

The use of natural fibers in construction materials is not recent. Over the decades and with countries industrialization, industrial materials have been developed and replaced traditional materials. However, with incentives to integrate sustainable development projects, there is a return to old materials and practices based on scientific researches.

In this context, the use of natural fibers in cement-based building materials has been a subject of interest of several studies such as [1-9].

A bibliographic synthesis of the formulation of cementitious composites with natural fibers of these articles is conducted and presented in table 1.

It is well known that the incorporation of natural fibers in a cement matrix influences the density and thermal conductivity. Usually, there is a decrease of thermal conductivity and density values with the increase of fibers fraction [10-15]. However, Wongsa *et al.* [9] showed that there is no significant impact of fibers amount on studied composites thermal conductivity. In fact, fibers volume fraction in this work did not exceed 1%.

Cementitious composites have relatively good compressive strength and weak tensile strength. The reinforcement of cementitious matrices with fibers allows the improvement of tensile strength, fracture toughness, material ductility and bridge the developed cracks [13,16,17,18]. Typically, the presence of fibers in composites does not improve the resistance to crack apparition, it influences the post-cracking behavior [19,20]. The strength increase is usually a few percent, but the toughness is highly increased.

The present research is focused on studying the effect the reinforcement of a cement paste with *Posidonia Oceanica* natural fibers. *Posidonia-Oceanica* is an aquatic Mediterranean plant from the *Posidoniaceae* family. In autumn, leaves and balls of *Posidonia-Oceanica* are

111 accumulated in beaches with various fragmentations. These debris are frequently eliminated
112 from beaches. Therefore, the valorization of this "waste product" in construction materials
113 seems interesting.
114 The use of fibers extracted from *Posidonia Oceanica* balls as an insulation material have been
115 studied in our previous work [21]. Results showed that these fibers could be used as a thermal
116 insulation material. Indeed, fibers thermal conductivity is close to the most commonly used
117 thermal insulation materials: thermal conductivity values are lying between 0.04 and 0.07
118 $W.m^{-1}.K^{-1}$. However, their heat capacity is significantly higher (about 2500 $J.kg^{-1}.K^{-1}$) [21].
119 In this work, the effect of the reinforcement of cement paste with *Posidonia Oceanica* fibers
120 is investigated. Table 1 was used to choose the studied composites formulation.
121 Allegue *et al.* [5] have studied the effect of the reinforcement of a cement paste with
122 *Posidonia-Oceanica* natural fibers on mechanical compressive and flexural strengths. This
123 reference is used to compare results found in this work concerning mechanical properties. The
124 originality of our paper consists in the study of thermal properties and the proposition of
125 analytical models to predict thermal and mechanical properties.
126 Thus, the present article is structured in the following way. Section 2 describes samples
127 preparation and characterization methods employed. Section 3 presents and discusses
128 experimental results. Analytical models to predict thermal and mechanical properties and a
129 comparison with experimental data are proposed and discussed in section 4. Section 5
130 summarizes our major conclusions.

131 *Table 1 : Synthesis of the composition of natural fibers reinforced cement matrices*

Matrix	***Fibers***	***Water/Cement***	***Volume fraction (%)***	***Fibers length (mm)***	***Chemical treatment***	***References***
Concrete	Sisal	0.57	1% à 5% (mass fraction)	50	None	[1]
Mortar	Sisal Coconut	0.4	3%	375 25	NaOH CaOH	[2]
Cement paste	Hemp	0.5	0 à 20%	20	None	[3]
Cement paste	Sisal Eucalyptus	N/A	1% à 5% (mass fraction)	1.66 0.66	None	[4]
Cement paste	Posidonia-Oceanica	0.5 à 1	0 à 20%	N/A	None	[5]
Cement paste	Flax	1	2%	25	- Rhéomac treated fibers - boiled fibers - Cement coated fibers	[6]
Mortar	Flax Hemp	0.5	1% to 3% (mass fraction)	16	Plasma	[7]
Mortar	Hemp	0.5	0 to 3%	6 - 12 - 18	None	[8]

			(mass fraction)			
Geopolymer mortar	Sisal Coconut	N/A	0%, 0.5%, 0.75%, and 1.0%	3.5 - 4	N/A	[9]

2. Experimental program

2.1. Samples preparation and microstructure

The studied composites were made of Portland cement paste CEM I 42.5 R and natural fibers of 1cm of length. Fibers were mechanically extracted from the marine Mediterranean plant *Posidonia-Oceanica* previously washed and dried. The water cement ratio is 0.5. Fibers volume fraction considered are 0, 5%, 10%, 15% and 20%.

Samples of 44×44×10 mm^3 were prepared for thermal tests and samples of 40×40×160 mm^3 for mechanical tests. Pre-notched samples with 8 mm tip width were prepared for fracture test. Three specimens were prepared for each group. All the specimens were demolded after 24h and conserved 28 days in the laboratory with recording of temperature and humidity. The temperature was about 20°C ± 2°C and the relative humidity was about 50% ± 5%.

Experimental results are obtained after hydration and results considered are obtained from the average of 3 samples. Thermophysical properties (density, thermal conductivity, thermal diffusivity and heat capacity) and mechanical properties (compressive strength, flexural strength and toughness) are evaluated and discussed.

SEM images of composites observed with JEOL 6301F scanning electron microscope are presented in Figure 1. As it can be seen, fibers of diameter of about 100 µm with a hollow structure are randomly dispersed in the cement paste. Additionally, as shown in Figure 2, some agglomerations of fibers are observed and lead to an additional porosity.

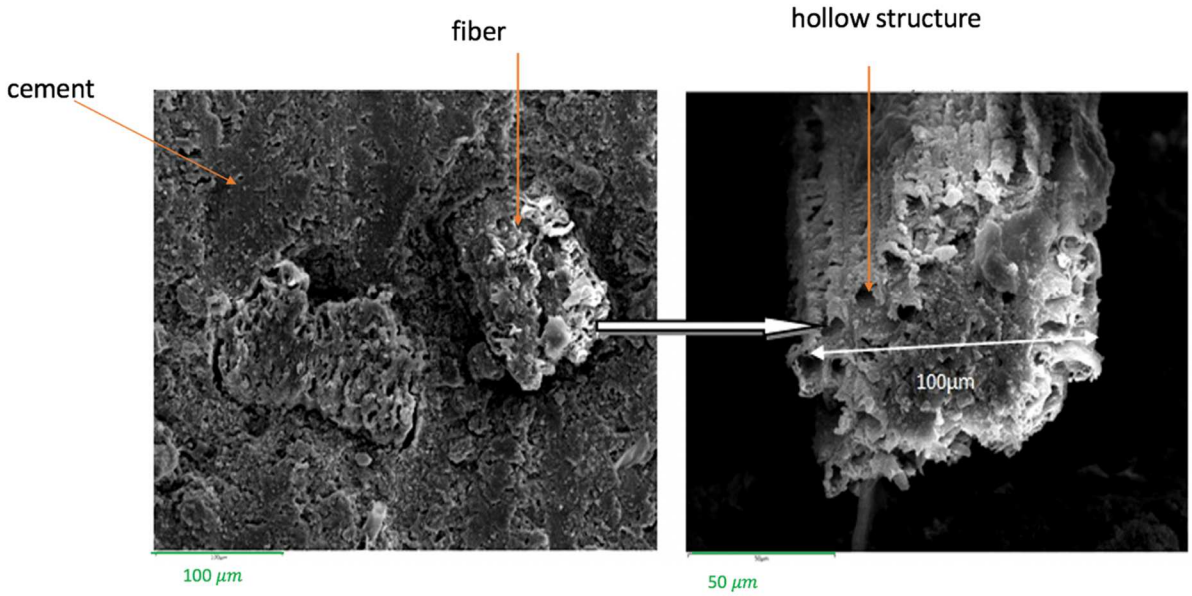

152

153 *Figure 1. SEM images for Posidonia-Oceanica fibers reinforced hardened cement paste ($\varphi = 5\%$)*

154

155

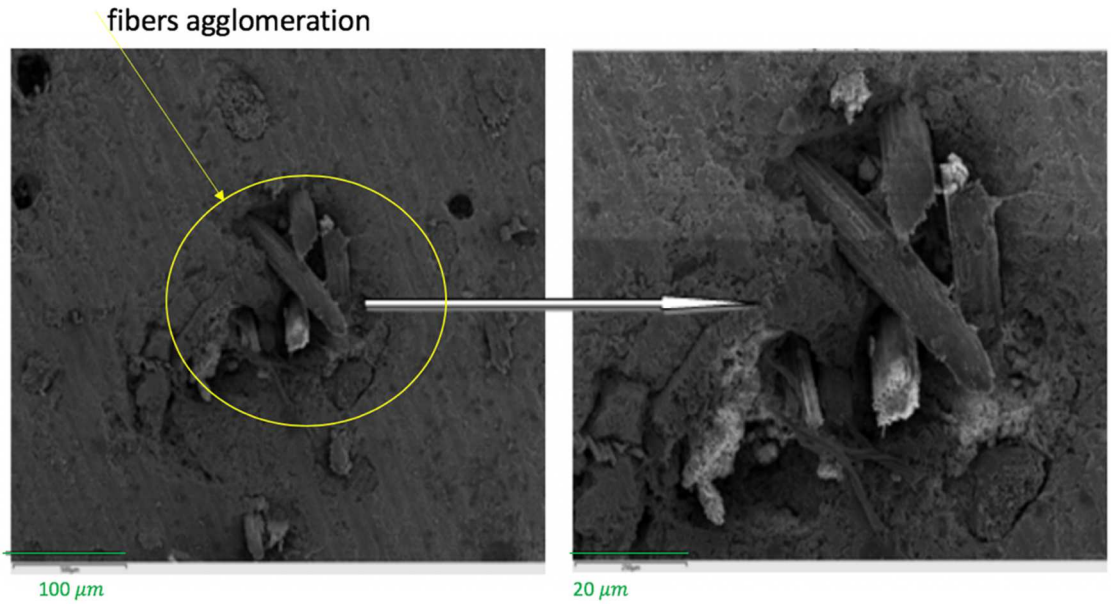

156

157 *Figure 2: SEM images of fibers agglomeration in Posidonia-Oceanica reinforced cement hardened*

158 *paste ($\varphi = 20\%$)*

159

2.2. Methods

2.2.1. Thermal tests

Thermal properties (thermal conductivity and thermal diffusivity) are measured with the Hot-Disk Transient Plane Source (TPS) method. This method consists in applying a controlled heat flux with a plane probe placed between two samples of the material to be tested. This probe is connected to the TPS device and acts as a heating source and a temperature sensor: the increase of the probe electrical resistance corresponding to the increase of its temperature is recorded.

More details concerning this method are available in a previous work [21] and in references [22-25].

In this work a TPS 2500 device is used. A probe (Reference 5465) with a radius of 3.189 mm is used. A heating power of 80 mW is applied during 20 s.

Repeatability measurements of thermal conductivity and thermal diffusivity with the Hot-Disk method have been carried out and showed that the standard deviation is about 4% for thermal conductivity measurements and 9% for thermal diffusivity [21]. These values are considered in the results of this study.

2.2.2. Mechanical tests

Mechanical tests are performed according to NF EN 12390 standard [26] and using an Universal Testing Machine FORM+TEST apparatus equipped with a 50 kN load cell. Samples of 40×40×160 mm^3 are horizontally placed upon two parallel supporting rollers spaced with 100 mm. A vertical load is applied in the middle of the sample with a constant speed of 50 $N.s^{-1}$. The load required to break the specimen F_f is recorded and the tensile strength obtained by flexural test is calculated as follows:

$$\sigma_{traction} = \frac{1.5 \times F_f \times L}{bw^2} \quad (1)$$

b, *w* are samples width and depth (*b* = 40 mm, *w* = 40 mm) and *L* is the span (*L*=120 mm). After failure prismatic beams used in flexural test are placed between two 40 × 40 mm^2 plates until rupture. The compressive strength is calculated from the failure load F_c and the sample area *A (A*=40 x 40 mm^2*)*.

The fracture toughness is determined according to ISO 12135 standard [27]. Pre-notched samples of size 40 × 40 ×16 mm^3 are placed in the flexural machine as shown in Figure 3.

Fracture toughness *Kc* is calculated as follows:

$$Kc = \frac{LP_f}{bw^{3/2}} f(\beta) \quad (2)$$

Where: *b = 40 mm*, *w = 40 mm* and *L* = 120 mm.

a is the notch length and P_f is the load required for rupture.

$$\beta = \frac{a}{w} \quad (3)$$

and

$$f(\beta) = \frac{3}{2}\sqrt{\beta}\,\frac{1{,}99 - \beta(1-\beta)(2{,}15 - 3{,}93\beta + 2{,}7\beta^2)}{(1+2\beta)(1-\beta)^{3/2}} \quad (4)$$

Figure 3. Notched beam specimen under flexural test

The average and the standard deviation of three samples are considered for mechanical properties.

3. Experimental results

3.1. Density

Samples density has been calculated from the average of the measurement of weight and volume of three samples.

Density variation as function of fiber volume fraction is presented in Figure 4. Results indicate that the material becomes slightly less dense with the increase of fibers volume fraction. Indeed, the density varies from 1761 kg.m^{-3} to 1613 kg.m^{-3}: a reduction of 8 % compared to the control cement paste is noted. This result is expected because of the hollow structure of fibers shown in SEM images of Figure 1 that generate voids and pores in the matrix. There is also an additional porosity coming from the fiber matrix interface and the fibers agglomeration (see Figure 2).

Composites density ρ_H as a function of fibers volume fraction φ could be written as follows:

$$\rho_H = \varphi\rho_f + (1-\varphi)\rho_m \quad (5)$$

Where ρ_f and $\rho_m$are respectively fibers and matrix densities.

Equation 5 allows the identification of ρ_m and ρ_f. Estimated densities are 1713 for ρ_m and 1214 kg.m^{-3} for ρ_f. A bibliographic synthesis was carried out by Pickering *et al.* [28] and showed that densities of natural fibers (Coir, Sisal, Hemp, Jute,) are situated between 1200 kg.m^{-3} and 1600 kg.m^{-3}.

This relashionship is available for samples including fibers. However, density founded for $\varphi=0$ is slightly lower than experimental measured density. This could be explained by fibers incorporation that tends increase matrix porosity.

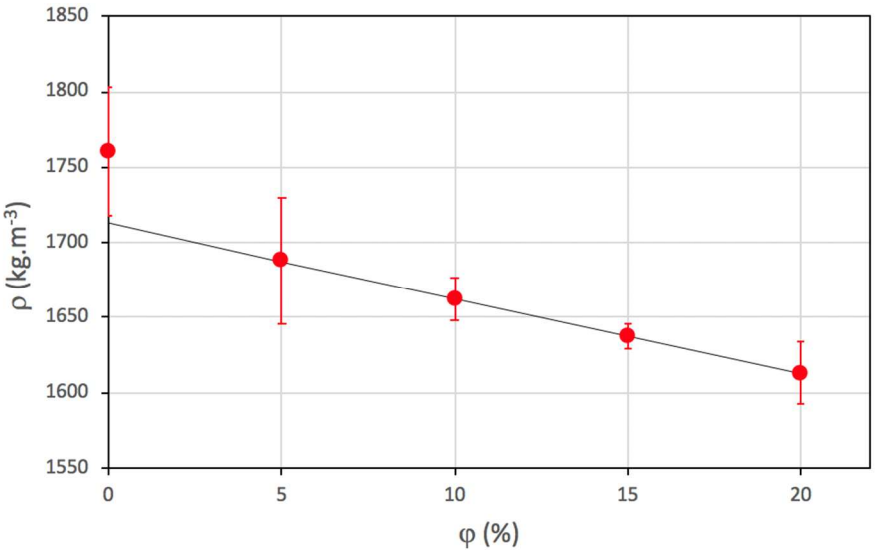

Figure 4. Samples density as function of fibers volume fraction

3.2. Thermal conductivity

Thermal conductivity values as a function of fibers volume fraction are presented in Figure 5. Cement composites containing *Posidonia-Oceanica* fibers thermal conductivity is varying from 0.718 W.m^{-1}.K^{-1} to 0.559 W.m^{-1}.K^{-1} for composites including 20% fibers volume fraction, thus showing a decrease of about 22% . This decrease could be explained by the density decrease and porosity increase that leads to reduce the heat transfer and the huge difference between fibers and matrix thermal conductivities: fibers thermal conductivity (k_f =

237 0.047 to 0.070 $W.m^{-1}.K^{-1}$) [21] is at least 10 times lower than that of the matrix (k_m = 0.718
238 $W.m^{-1}.K^{-1}$). In addition, the fibers incorporation in the matrix creates many interfaces that
239 act as thermal contact resistances and leads to a decrease in thermal conductivity. This
240 result has been also reported by many researches. Benmansour *et al.* [12] in their study of
241 the development of an insulation material made of mortar including date palm fibers.
242 Authors have noted a decrease of 92.5% in thermal conductivity values. This important drop
243 compared to our results is due to the fibers content tested that reaches 30% weight fraction.
244 Belhaj *et al.* [13] have noted a decrease from 1.4 $W.m^{-1}K^{-1}$ to 1.32 $W.m^{-1}K^{-1}$ on thermal
245 conductivity values of barley straw reinforced cement. Onésippe *et al.* [14] have reported
246 that thermal conductivity decreases from 0.62 $W.m^{-1}K^{-1}$ to 0.46 $m^{-1}K^{-1}$ with the introduction
247 of Bagasse fibers in a cement-based matrix. Same ascertainments have been noticed by
248 Akinyemi *et al.* [15] in their work concerning the incorporation of banana fibers and wood
249 bottom ash in a cement matrix.
250 In addition, samples thermal conductivity relative variation as a function of the density
251 relative variation presented in Figure 6 shows that there is a correlation between these two
252 properties. This result confirms those already observed by Ibos [29] for other natural fibers
253 used in the reinforcement of organic or mineral matrices.

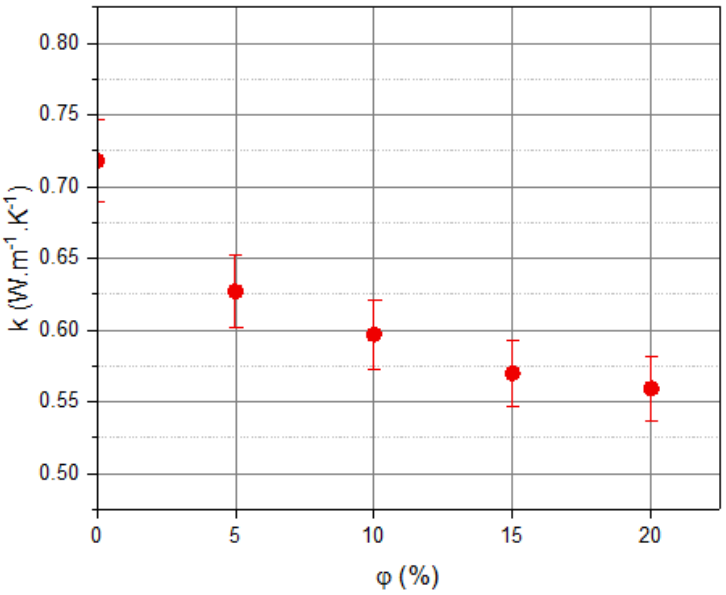

254

255 *Figure 5. Samples thermal conductivity as function of fibers volume fraction*

256

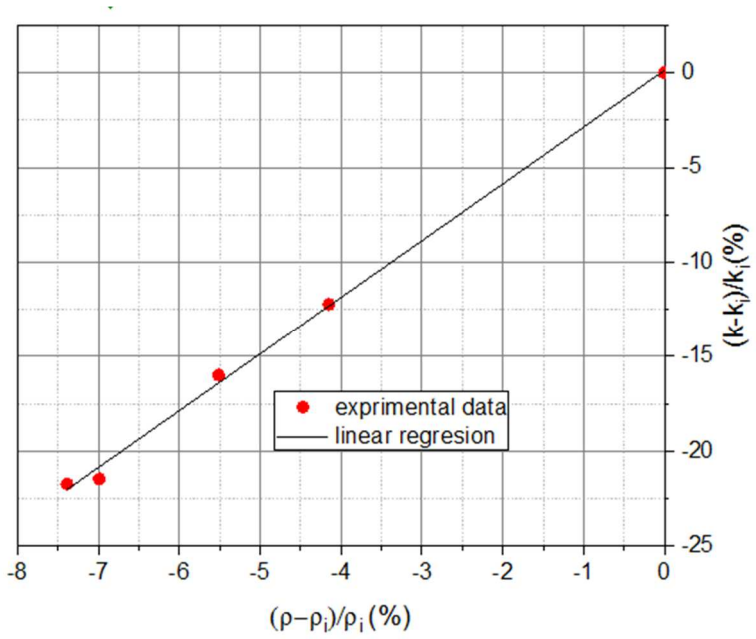

257

258 *Figure 6. Composites thermal conductivity relative variation as a function of density relative*

259 *variation: effect of fiber content*

260

261 **3.3. Thermal diffusivity**

As shown in Figure 7, samples thermal diffusivity is ranging between 0.362 × 10^{-6} $m^2.s^{-1}$ and 0.298 × 10^{-6} $m^2.s^{-1}$. Thermal diffusivity decreases very slightly with the incorporation of fibers in the cement matrix. A decrease of 12% is observed from the introduction of 5% of fibers. However, non-significant variation is noted for higher fibers volume fractions, regarding measurement uncertainties. Therefore, it could be reported that *Posidonia-Oceanica* fibers introducing in cement matrix plays a minor influence on thermal diffusivity. Onésippe *et al.* [14] have calculated thermal diffusivities of their Bagasse fibers reinforced cement composites from their thermal conductivity, density and heat capacity measurements. Thermal diffusivities found in their study do not show important variation and are lying between 1.18× 10^{-6} $m^2.s^{-1}$ and 1.58 × 10^{-6} $m^2.s^{-1}$.

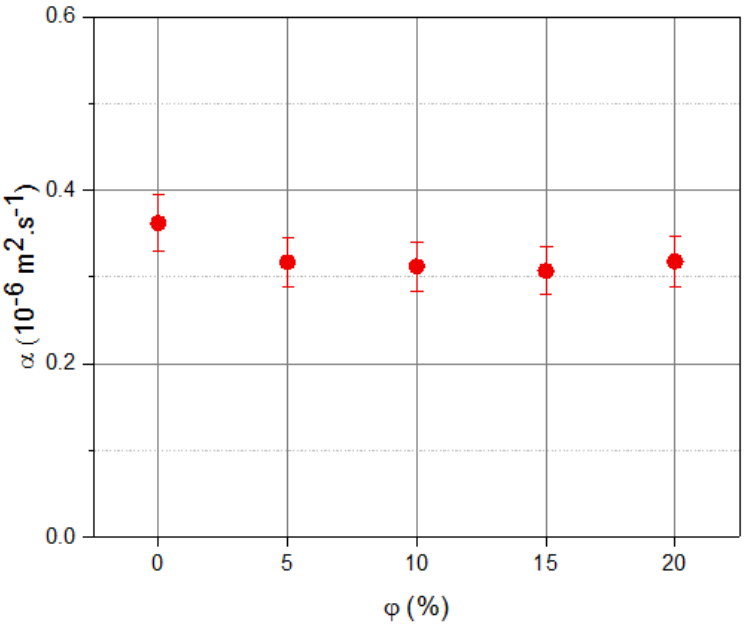

Figure 7. Samples thermal diffusivity as function of fibers volume fraction

3.4. Flexural strength

Flexural strength is the tensile strength obtained by flexural test and estimated by Equation 1. Flexural strength as a function of fibers volume fraction is presented in Figure 8.

Results revealed that flexural strength increases by 27% for the composites including 5% of fibers compared to the cement paste. For higher fibers volume fraction, flexural strength decreases but still remains higher than the control cement paste strength. Fibers presence in a cementitious matrix improves the composite tensile and allows crack bridging. For higher fiber content, mixing becomes difficult and composites homogeneity is affected by fibers agglomeration. Allegue *et al.* [5] have reported the same behavior of their composites made of a cement matrix with *Posidonia-Oceanica* fibers. Flexural strengths for composites with 0.5 W/C ratio were found between 4.3 MPa and 5.6 MPa. The slight difference compared to our results could be associated to the difference between the type of cement used. Sedan *et al.* [3] have revealed the same trend in their study of a cement matrix reinforced with hemp fibers. For fiber contents varying from 0 to 20% and a W/C ratio of 0.5, authors noted flexural strength values between 4 MPa and 6.8 MPa. Belhaj *et al.* [13] have noticed an increase of 6% and a decrease of 6% compared to the control samples when adding respectively 5 $kg.m^{-3}$ and 15 $kg.m^{-3}$ of barley straws.

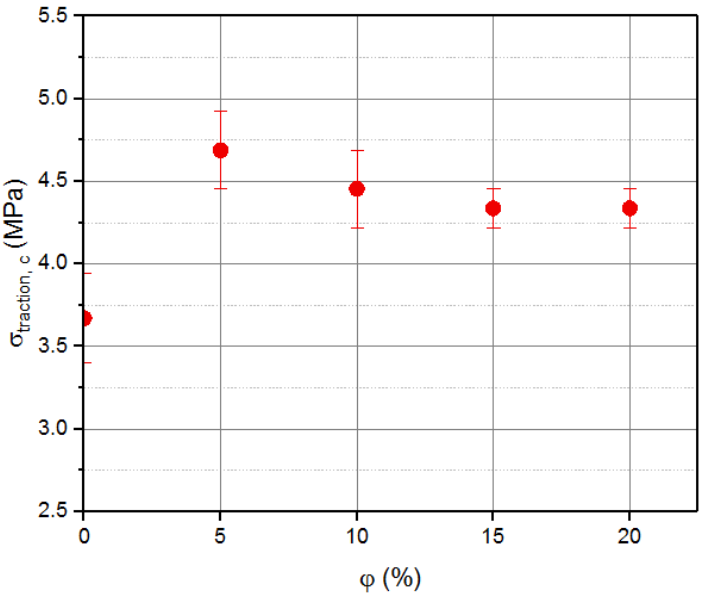

Figure 8. Samples flexural strength as function of fibers volume fraction

294

295 **3.5. Compressive strength**

296 Samples compressive strength as a function of fibers content is presented in Figure 9. Results
297 revealed that compressive strength has the same behavior than tensile strength obtained by
298 flexural test: it increases with the addition of fibers then it decreases then but still higher than
299 the control cement strength. The peak corresponding to a 27% of strength increase is obtained
300 at 10% of fibers volume fraction. This decrease could be associated to the rise of composite
301 porosity. However, the optimal compression strength is obtained for 10% of fibers volume
302 fraction. A similar behavior was also reported by Allegue *et al.* [5]. Zaroudi *et al.* [30] also
303 reported such a variation in a study concerning the use of polyolefin fiber on an eco-friendly
304 concrete. Authors indicated that there is a slight rise of compressive strength values with the
305 introduction of 0.5 kg.m^{-3} of fibers, and a decrease is observed for higher fibers content.
306 However, Benmansour *et al.* [12] have observed a substantial decrease of compressive
307 strength when increasing date palm fibers fraction in mortar.

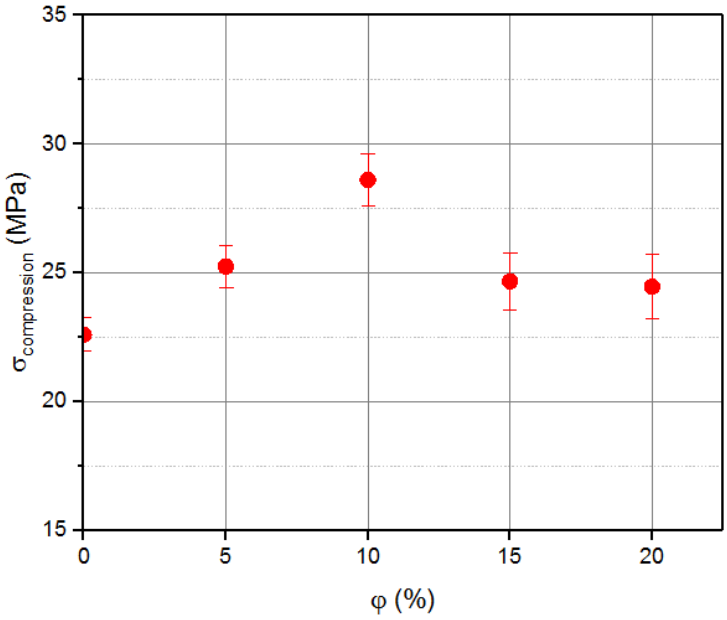

308

309 *Figure 9. Samples compressive strength as function of fibers volume fraction*

3.6. Toughness

Fracture toughness variation as a function of fibers volume fraction is presented in Figure 10. A linear and significant increase of toughness is observed with the increase of fibers content. An increase of 65% is observed for composites including 20% of fibers. Thus, it could be deduced that the addition of fibers significantly improves the material toughness and therefore its resistance to cracks propagation. This leads to the decrease of the material brittleness and of its ductility due to the role of fibers in the bridging of cracks. Fibrous composites crack bridging is owing to the presence of frictional shear resistance along the interface between fibers and matrix [31]. Similar results have been reported for cement-based composites with natural or synthetic fibers by Banthia *et al.* [17,18], Fu *et al.* [19], Mohr et *al.* [32] Juarez *et al.* [33], Akhavan *et al.* [34], Bekhiti *et al.* [35] and Wang *et al.* [36].

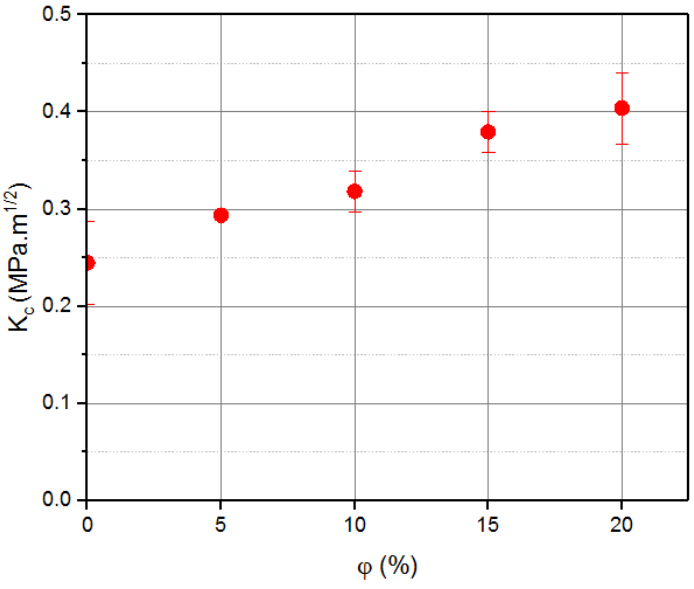

Figure 10. Samples toughness as function of fibers volume fraction

4. Analytical models

4.1. Hypothesis, microstructure and geometrical model

Several approaches and models to predict the mechanical and thermal properties of short fiber composites are available in the literature. It is well known that composites properties are dependent to fibers shape, length, orientation and the fiber-matrix interface [37,38].

Based on the experimental data and assuming some simplifying hypothesis chosen from composites microstructure, simplified models were developed to predict thermal conductivity, tensile and compressive strengths and fracture toughness as a function of fibers volume fraction.

In order to predict composites properties, the following simplifying hypotheses are considered:

- fibers are cylindrical with an average diameter of 100 μm (see SEM images of Figure 1);
- fibers are of average 10 mm length (measured with a caliper);
- fibers are considered uniformly distributed in the matrix;
- fibers are horizontally oriented in the matrix;
- for thermal model, heat flux is considered perpendicular relatively to fibers arrangement and for mechanical model load direction is in the same direction of fibers. These two configurations are chosen because they correspond to the expected application of these materials as a construction material. Measurements were performed accordingly to these hypotheses.
- It was observed from SEM images of composites (see Figure 2) that fibers tend to agglomerate. This phenomenon depends on fibers volume fraction. Thus, an effective diameter d of the fibers as a function of the volume fraction could be defined. d is the diameter of inclusion which represents an agglomeration of fibers or a distributed single

fibers for low volume fractions of fibers. The effective diameter d is considered linearly increasing as a function of fibers volume fraction:

$$d = d_0 + 20\varphi d_0 \quad (6)$$

Where d_0 is the fiber diameter (100 μm) and φ is the ratio of fibers fraction.

This is an empirical relationship chosen from SEM images. In fact, for a composite with 20% of fibers it could be observed that a bundle of five fibers is formed. The effective diameter d is then 500 μm in this case.

Assuming the simplified hypotheses presented above, the geometric model considered for the analytical predictions is presented in Figure 11.

Inclusion distribution in the matrix considered for analytical model and the simplified representative volume element (RVE) corresponding to a half-cylindrical fiber included in a cement parallelepiped are presented in Figures 11 and 12.

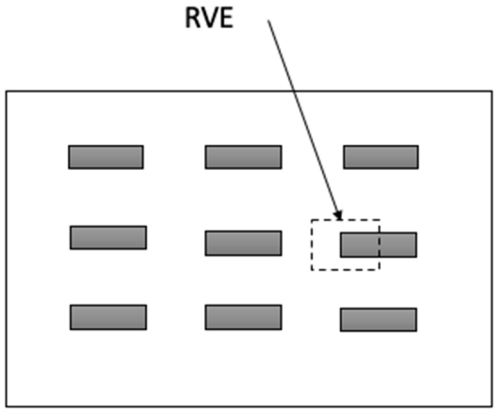

Figure 11. Simplified repartition of inclusions in the matrix

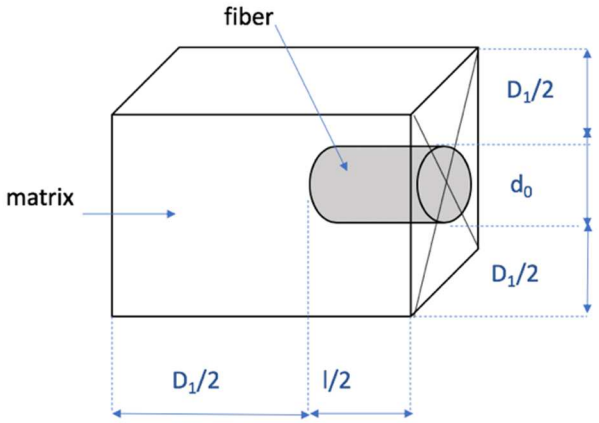

Figure 12. Elementary representative volume of composite V_0

Three variables ε, γ, and δ are defined such as:

$$\varepsilon = \frac{D_1}{l} \tag{7}$$

$$\gamma = \frac{D_1}{D_2} \tag{8}$$

$$\delta = \frac{l}{d_0} \tag{9}$$

γ is assumed equal to 50 (the same ratio between fibers mi-length 5 mm and diameter 100 μm).

Cylindrical fiber (of length l and diameter d_0) is then replaced as shown in Figure 13 by an equivalent parallelepiped of same length and volume. The square section of this "equivalent" fiber is $d_0'^2$. Thus, we obtain:

$$\frac{\pi d_0^{\,2}}{4} \times \frac{l}{2} = d_0^{\,'2} \times \frac{l}{2} \Leftrightarrow d_0^{\,'} = d_0 \frac{\sqrt{\pi}}{2} \tag{10}$$

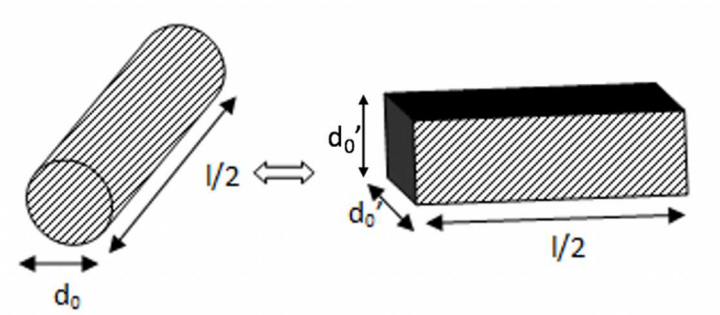

Figure 13. Inclusions modeling

The modified representative volume element V_1 is presented in Figure 14. The heat flow direction considered is also presented. The surface projection of the RVE for thermal and mechanical models are respectively shown in Figures 15 and 16. This RVE is then divided into sub-volumes. Equivalent volume fractions (φ_{p1}, φ_{s1} *and* φ_{p1}') for each volume are defined. The volume V_1 is composed of a cement parallelepiped in parallel with a volume V_2 relatively to the heat flow direction. V_2 is composed of a fiber parallelepiped in a cement parallelepiped as shown in Figure 17. Therefore, a 'parallel' volume fraction φ_{p1} could be defined as follows:

$$\varphi_{p1} = \frac{l}{l+D_1} = \frac{1}{1+{}^{D_1}/_{l}} = \frac{1}{1+\varepsilon} \tag{11}$$

Where l is the average length of fibers, D_1 is the horizontal distance between fibers.

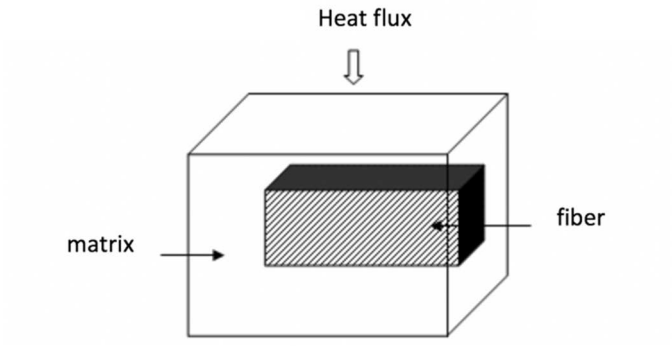

Figure 14. Modified representative volume element V_1

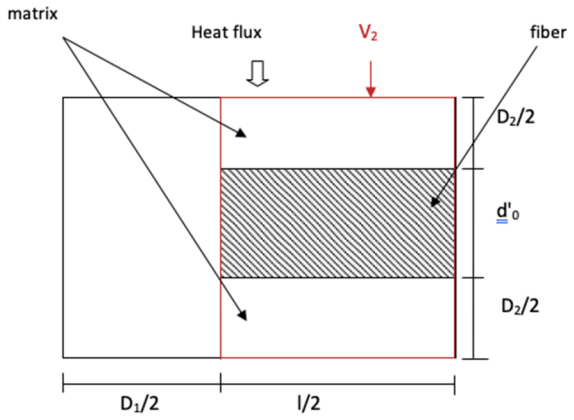

Figure 15. Geometrical thermal model projection

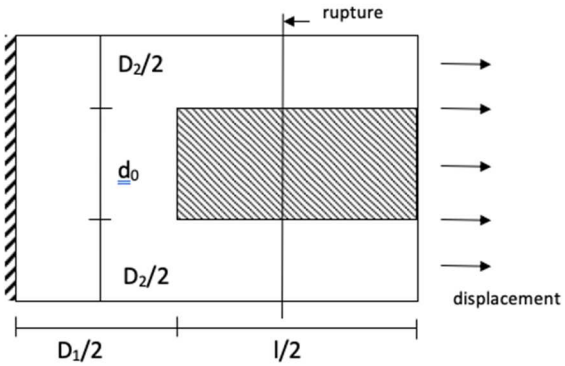

Figure 16. Geometrical mechanical model projection

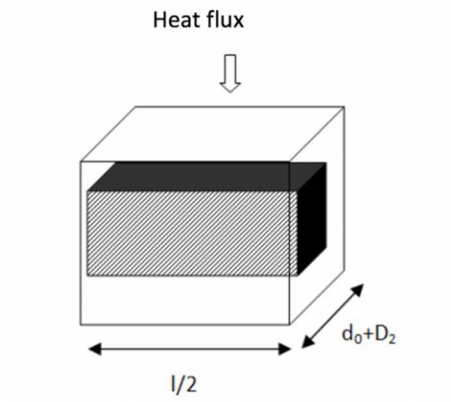

Figure 17. Representative volume element V_2

The RVE V_2 is then subdivided into two volumes: a volume corresponding to the matrix in series with a volume V_3 where V_3 is a parallelepiped of fiber embedded in a cement

parallelepiped as shown in Figure 18. A 'series' fibers volume fraction φ_{s1} is determined considering the volume V_2 and defined as follows:

$$\varphi_{s1} = \frac{d'_0}{d'_0+D_2} = \frac{\sqrt{\pi}d_0}{\sqrt{\pi}d'_0+2D_2} = \frac{1}{1+\frac{2}{\sqrt{\pi}}\times\frac{\varepsilon\delta}{\gamma}} \quad (12)$$

'Parallel' fibers volume fraction φ_{p1}' could be defined with considering the volume V_3 (see Figure 18) as follows:

$$\varphi'_{p1} = \frac{d'_0}{d'_0+D_2} = \frac{\sqrt{\pi}d_0}{\sqrt{\pi}d'_0+2D_2} = \frac{1}{1+\frac{2}{\sqrt{\pi}}\times\frac{\varepsilon\delta}{\gamma}} = \varphi_{s1} \quad (13)$$

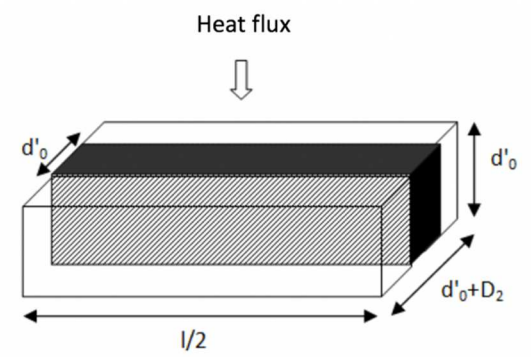

Figure 18. Elementary representative volume V_3 for thermal model

Finally, total fibers volume fraction φ is:

$$\varphi = \varphi_{p1} \times \varphi_{s1} \times \varphi_{p1}{}' \quad (14)$$

To determine distances D_1 and D_2, Equation 14 is considered. φ_{p1}, φ_{s1} and $\varphi_{p1}{}'$ are respectively replaced by their formulas of Equations (11), (12) and (13). Variables ε, γ, and δ are then used to find D_1 and D_2.

It amounts to solve for each fibers volume fraction φ the following degree 3 Equation:

$$\varphi\delta^2\varepsilon^3 + \varphi\delta(\delta+2)\varepsilon^2 + (2\delta+1)\varphi\varepsilon + 1 - \varphi = 0 \quad (15)$$

We recall that for a given volume fraction, parameters δ and γ are known (see Equations 8 and 9). Thus, solving Equation 15 allows the determination of ε. RVE dimensions D_1 ($D_1 = \varepsilon \times l$) and D_2 ($D_2 = \frac{D_1}{\gamma}$) are then calculated.

The variation of effective fibers diameter d calculated with Equation 6 and results of the estimated horizontal and vertical distances between fibers D_1 and D_2 are presented in Figure 19 as a function of fibers volume fraction φ.

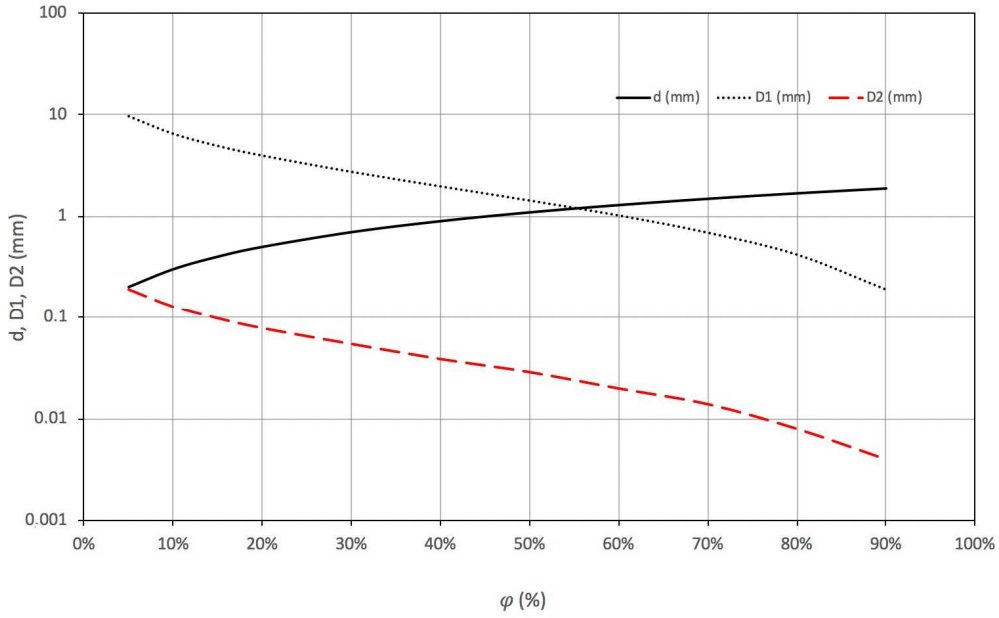

Figure 19. Distances d, D_1 and D_2 as a function of fibers volume fraction

4.2. Thermal model

The equivalent thermal conductivity k_H of the composite could be written by considering the RVE V_1 as a function of the volume fraction φ_{p1} given by Equation 11, the matrix thermal conductivity k_m and the thermal conductivity of the volume V_2 k_{h1}:

$$k_H = \varphi_{p1} k_{h1} + (1 - \varphi_{p1}) k_m \quad (16)$$

k_{h1} is calculated on the basis of Equation 17 using the volume fraction φ_{s1}, the matrix thermal conductivity k_m and k_{h2} the thermal conductivity of the volume V_3.

438 $$\frac{1}{k_{h1}} = \frac{\varphi_{s1}}{k_{h2}} + \frac{(1-\varphi_{s1})}{k_m} \quad (17)$$

439 k_{h2} is calculated on the basis of Equation 18 using the volume fraction $\varphi_{p1'}$, the matrix
440 thermal conductivity k_m and fiber*s* thermal conductivity k_m.

441 $$k_{h2} = \varphi_{p1}' k_f + (1-\varphi_{p1}')k_m \quad (18)$$

442

443 ***4.3. Comparison between thermal conductivity model and experimental results***

444 The experimental measurements of thermal conductivity are compared to the upper and the
445 lower bounds given by the first order thermal models. These models allow to define for a
446 composite material the lower bound k_{inf} and the upper bound k_{sup} of thermal conductivity k.
447 Assuming that the composite is a multi-layers material, the lower bound is giving by
448 considering a series assembly of the material layers relatively to the heat flow direction. The
449 upper bound is given by considering a parallel assembly of fibers and matrix relatively to the
450 heat flow.

451 For a two homogenous layers material, k_{inf} and k_{sup} thermal conductivity limits are written as a
452 function of the fibers volume fractions φ and fibers and matrix thermal conductivities k_f and
453 k_m as follows [37]:

454 $$\frac{1}{k_{\inf}} = \frac{(1-\varphi)}{k_m} + \frac{\varphi}{k_f} \quad (19)$$

455 $$k_{\sup} = (1-\varphi)k_m + \varphi\, k_f \quad (20)$$

456 k_m is the hardened cement paste without fibers thermal conductivity (k_m = 0.718 $W.m^{-1}.K^{-1}$)
457 and k_f is *Posidonia-Oceanica* fibers thermal (k_f = 0.070 $W.m^{-1}.K^{-1}$) corresponding to fibers
458 maximal thermal conductivity measured in a previous work [21].

459 Figure 20 illustrates a comparison between the experimental values of thermal conductivity
460 and the model developed in part 4.2. The experimental and proposed model values are

461 ranging between lower and upper limits of series and parallel models. The model developed
462 to estimate thermal conductivity has the same variation of experimental measurements.

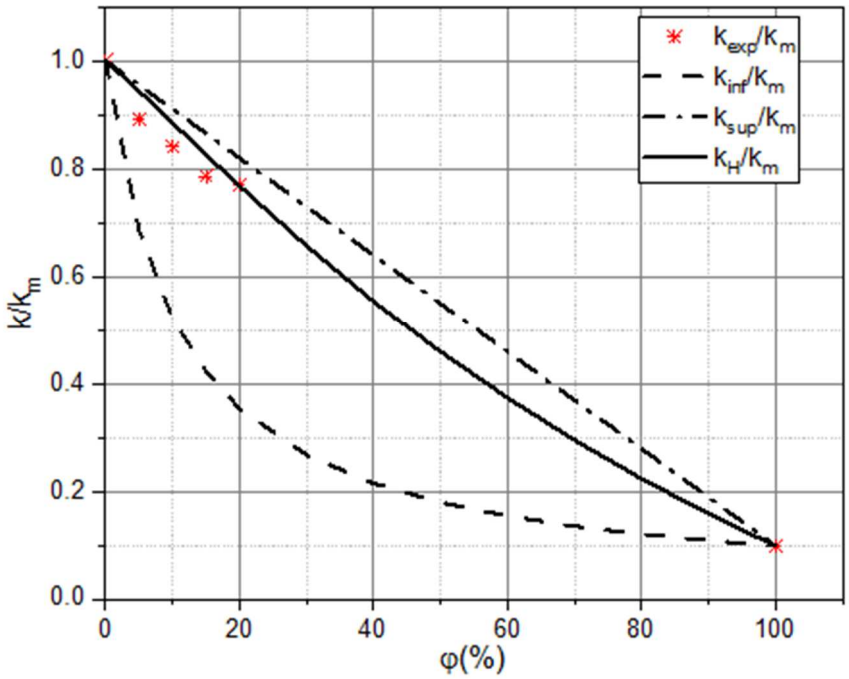

463

464 *Figure 20. Comparison between experimental and analytical thermal conductivities*

465

4.4. Mechanical model

Fibrous composites failure is depending on fiber matrix interface. Matthews *et al.* have reported that two modes of failure are possible [39]: fibers rupture or fibers sliding.

Figure 19 presents a part of composite after flexural test. It could be observed by examining the rupture surface of composites that fibers are undamaged. Therefore, it could be assumed that

rupture occurs rather by fibers sliding at fiber-matrix interface.

The corresponding geometric model is shown in Figure 16.

The composite tensile strain $\sigma_{traction,c}$ is defined as a function of the interface shear strength τ, the matrix tensile strain $\sigma_{traction,m}$, the geometric properties of the fiber l and d and the fiber volume fractions φ.

According to Matthews *et al.* [39] and Van Hattum *et al.* [40], the tensile strain is given by Equation 21 where d is the agglomerated fibers diameter supposed variable as a function of fibers volume fraction.

$$\sigma_{traction,c} = \varphi \times \frac{\tau \times l}{2d} + (1-\varphi) \times \sigma_{traction,m} \quad (21)$$

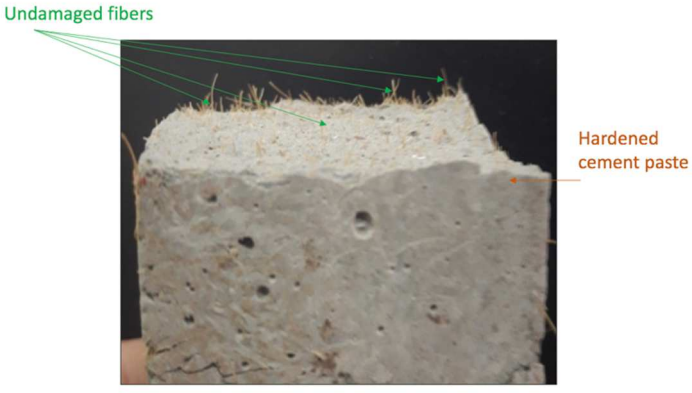

Figure 21. Composite specimen fractured surface observed after flexural test (rupture by fibers sliding)

4.5. Tensile and compressive strengths models and comparison with experimental results

Equation 15 is considered in order to determine the tensile strength variation as a function of fibers volume fraction. The effective diameter d is replaced by Equation 6, Equation 21 becomes:

$$\sigma_{traction,c} = \varphi \times \frac{\tau \times l}{2(d_0 + 20\varphi d_0)} + (1-\varphi) \times \sigma_{traction,m} \quad (22)$$

The value of the interface shear strength is estimated by model identification with experimental data. A value of τ of 0.328 MPa is identified. Figure 22 presents a comparison of experimental tensile strengths with the analytical model previously presented. The tensile strength is increasing until a maximal strength corresponding to optimal amount fibers fraction in the cement matrix. Above this value, strength decreases.

In order to determine the direct tensile strength $\sigma_{traction,T}$ from tensile strength obtained by flexion $\sigma_{traction,c}$, the CERIB (Centre d'Etudes et de Recherches de l'Industrie du Béton) proposed the following formula [41]:

$$\sigma_{traction,T} = 0.6\sigma_{traction,c} \quad (23)$$

Compressive strength and tensile strength are correlated by the following relationship [42,43]:

$$\sigma_{compression,c} = f\sigma^{g}{}_{traction,T} \quad (24)$$

Where f and g are two constants to be determined by model identification with experimental measurements.

$\sigma_{traction,T}$ of the Equation 24 is replaced by Equation 23. $\sigma_{traction,c}$ is then replaced by Equation 22, $\sigma_{compression,c}$ becomes:

505 $$\sigma_{compression,c} = 0.6 f\left(\varphi \times \frac{\tau \times l}{2(d_0 + 20\varphi d_0)} + (1-\varphi) \times \sigma_{traction,m}\right)^g \quad (25)$$

506 Coefficients *f* and *g* are estimated by model fitting with experimental results. Values found
507 are 8.46 for *f* and 1.1 for *g*. The interface shear strength τ taken is 0.328 MPa (value found in
508 section 4.5). The model of compressive strength is then plotted in Figure 23 and compared to
509 measured compressive strengths. It can be easily seen that both model and experimental data
510 have the same trend: there is an increase of composite compressive strength with fiber
511 incorporating until a maximum value. Then, for higher fiber volume fractions, the
512 compressive strength decreases. Classical models did not predict this variation of strength. It
513 has been demonstrated through this simplified model that this behavior is due to fibers
514 agglomeration for high fibers content.

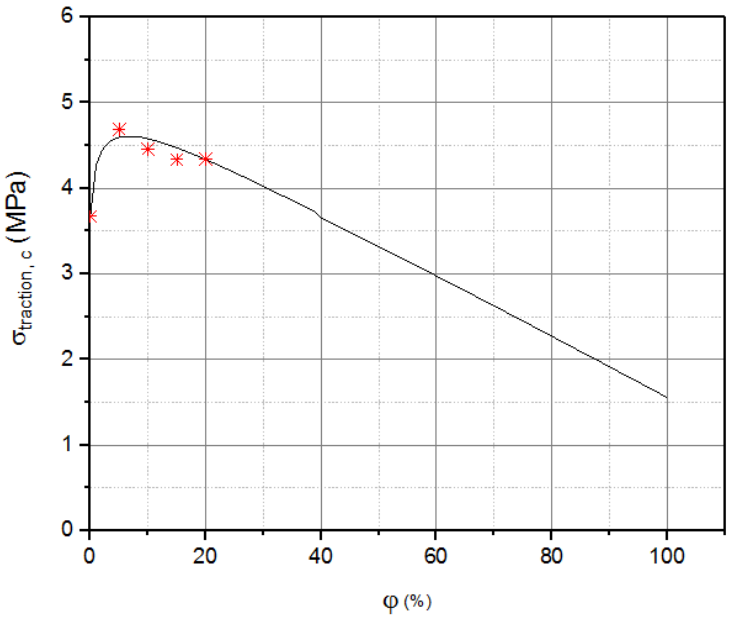

515

516 *Figure 22. Comparison between experimental and analytical tensile strengths*

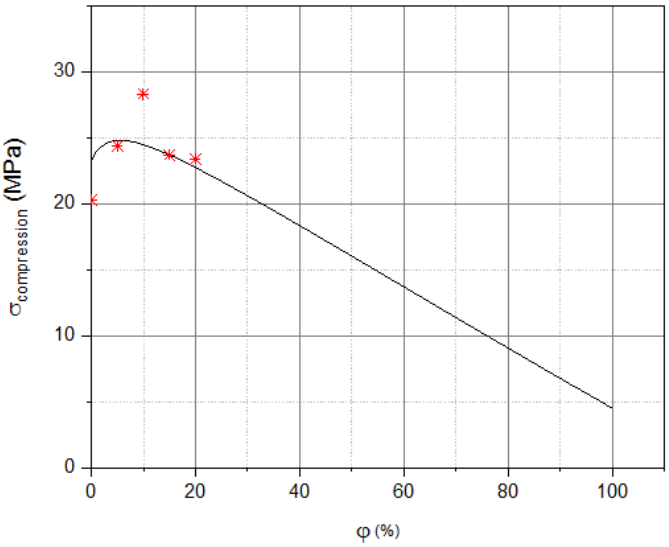

517

518 *Figure 23. Comparison between experimental and analytical compressive strength*

519

520 ***4.6. Toughness* model and comparison with experimental results**

521 In this section rupture energy of an homogenized RVE is considered. Fracture toughness
522 could be written as a function of the fracture energy *Gc* and Young's modulus *Ec* by in the
523 following way [39]:

524 $$K_c = \sqrt{E_c G_c} \tag{26}$$

525 The homogenized composite fracture energy *Gc* can be expressed as a function of the rupture
526 energy in the volume part containing the matrix G_m and the fracture energy of the part
527 containing a part of fiber and matrix *G'*.

528 $$G_c.S = G_m.S + G'.2\pi d\frac{l}{2} \tag{27}$$

529 Where *S* is the area of dimensions $(d + D_2)^2$ (see Figure 16).

530 The fracture energy *Gc* becomes:

531 $$G_c = G_m + G'\frac{\pi dl}{(d + D_2)^2} \tag{28}$$

532 Furthermore, Young's modulus can be written according to the law of mixing as follows:

533 $$E_c = \varphi.E_f + (1-\varphi).E_m \quad (29)$$

534 *Gc* is replaced by Equation 28, *Ec* by Equation 29 and *d* by Equation 6.

535 It follows that equation 27 becomes:

536 $$K_c = \sqrt{(\varphi.E_f + (1-\varphi).E_m).(G_m + G'\frac{\pi(d_0 + 20\varphi d_0)l}{(d_0 + 20\varphi d_0 + D_2)^2})} \quad (30)$$

537

538 According to Haecker *et al.* [44], Young's modulus of Portland cement paste with 0.5
539 water/cement ratio is 20 GPa. The fracture energy of the matrix G_m is estimated from the
540 matrix experimentally determined fracture toughness and cement paste young modulus.
541 *Posidonia-Oceanica* fibers Young's modulus E_f, fracture energy in the volume containing the
542 fiber and the matrix *G'* are estimated by reducing the gap of uncertainties between the model
543 and the experimental data. D_2 is considered variable as a function of fibers volume fraction φ
544 and calculated as shown in section 4.1. *G'* identified is about 90 $N.m^{-1}$. E_f is about 100 GPa,
545 E_f could be accepted because according to literature natural fibers Young's modulus is
546 varying from 6 to 130 GPa [45] and [46].
547 Figure 24 illustrates the developed model of fracture toughness *Kc* variation as a function of
548 fibers volume fraction compared to experimental results. It can be easily observed that the
549 proposed model has the same variation with experimental data for fiber content ranging
550 between 0% and 20% and that fracture toughness is increasing with fibers volume fraction
551 increase. It confirms that fibers incorporating in a cement brittle matrix improves its ductility.

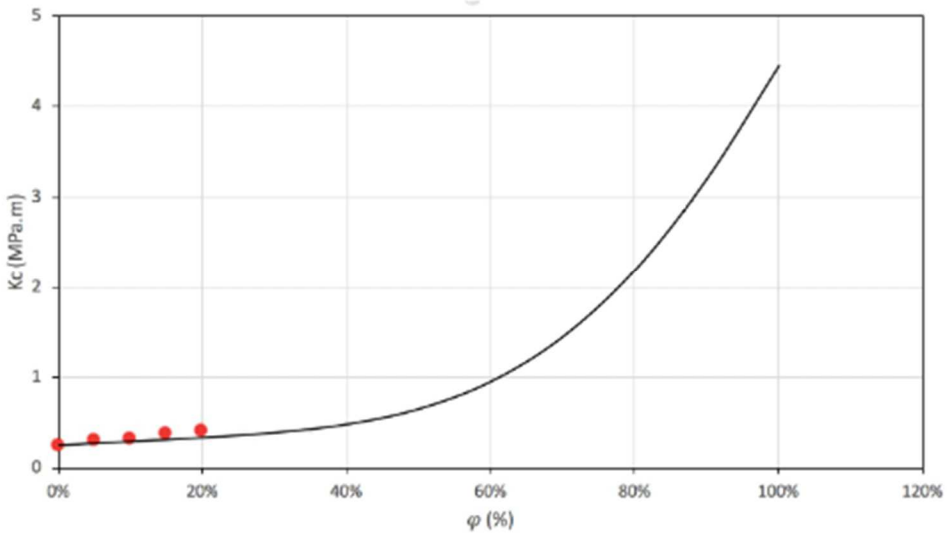

Figure 24. Experimental and analytical fracture toughness of composites as function of fibers volume fraction

5. Conclusion

This study investigated the reinforcement of cement paste with *Posidonia-Oceanica* natural fibers. The effect of fibers volume fraction variation on composites thermal and mechanical preparties had been studied. *Posidonia-Oceanica* fibers volume fraction considered have been varied from 0 to 20%. It was found that fibers volume fraction increase allows the improvement of the material insulation properties: thermal conductivity values have decreased of about 22% with the use of about 20% of fibers volume fraction. An analytical model de predict the thermal conductivity as a function of volume fraction has been also developed. This model was compared to experimental data between 0 and 20% fibers volume fraction.

Composites mechanical properties have been measured and analytical models were defined to predict composites compressive, tensile strengths and fracture toughness as a function of fibers volume fractions. It was observed that compressive and flexural strengths increased of about 27% between 5% and 10% then decreased but still higher than specimens without

fibers. However, it appears that fracture toughness was significantly increased with the increase of fibers fraction. Analytical models for variation of compressive and tensile strengths and fracture toughness have been also developed and compared to experimental data. It was shown that the pic observed in compressive and tensile strengths is due to fibers agglomeration for high volume fraction. It was also shown that fibers incorporating in this cementitious matrix increases significantly the material ductility and his ability to bridge cracks.

As a result of this research, the use of natural fibers of *Posidonia-Oceanica* in the reinforcement of a cement matrix seems an interesting application for their valorization in the construction domain. Material thermal and mechanical properties could be improved. This improvement depends on fibers quantity which depends on the intended application. If a maximal strength is needed fibers volume fraction should preferably not exceed 10% and if the priority is having maximal ductility and/or good insulation properties, fibers volume fraction could be higher.

Moreover, models developed in this work could give an estimation of thermal conductivity, fracture toughness and compressive and tensile strengths as a function of any *Posidonia-Oceanica* fibers volume fraction.

References

[1] Swift, D. G., & Smith, R. B. L. (1978, August). Sisal fibre reinforcement of cement paste and concrete. In *Proc. Int. Conf. on Materials of Construction for Developing Countries. Asian Inst. of Tech., Bangkok* (pp. 193-198).

[2] Tolêdo Filho, R. D., Scrivener, K., England, G. L., & Ghavami, K. (2000). Durability of alkali-sensitive sisal and coconut fibres in cement mortar composites. *Cement and concrete composites*, *22*(2), 127-143.

[3] Sedan, D., Pagnoux, C., Smith, A., & Chotard, T. (2007, August). Propriétés mécaniques de matériaux enchevêtrés à base de fibre de chanvre et matrice cimentaire. In *Congrès français de mécanique*. AFM, Maison de la Mécanique, 39/41 rue Louis Blanc-92400 Courbevoie.

[4] Roma Jr, L. C., Martello, L. S., & Savastano Jr, H. (2008). Evaluation of mechanical, physical and thermal performance of cement-based tiles reinforced with vegetable fibers. *Construction and Building Materials*, *22*(4), 668-674.

[5] Allegue, L., Zidi, M., & Sghaier, S. (2015). Mechanical properties of Posidonia oceanica fibers reinforced cement. *Journal of Composite Materials*, *49*(5), 509-517.

[6] Sawsen, C., Fouzia, K., Mohamed, B., & Moussa, G. (2015). Effect of flax fibers treatments on the rheological and the mechanical behavior of a cement composite. *Construction and Building Materials*, *79*, 229-235.

[7] Fantilli, A. P., Chiaia, B., & Gorino, A. (2016). Fiber volume fraction and ductility index of concrete beams. *Cement and Concrete Composites*, *65*, 139-149.

[8] Çomak, B., Bideci, A., & Bideci, Ö. S. (2018). Effects of hemp fibers on characteristics of cement based mortar. *Construction and Building Materials*, *169*, 794-799.

[9] Wongsa, A., Kunthawatwong, R., Naenudon, S., Sata, V., & Chindaprasirt, P. (2020). Natural fiber reinforced high calcium fly ash geopolymer mortar. *Construction and Building Materials*, *241*, 118143.

[10] Khedari, J., Watsanasathaporn, P., & Hirunlabh, J. (2005). Development of fibre-based soil–cement block with low thermal conductivity. *Cement and concrete composites*, *27*(1), 111-116.

[11] Bentchikou, M., Guidoum, A., Scrivener, K., Silhadi, K., & Hanini, S. (2012). Effect of recycled cellulose fibres on the properties of lightweight cement composite matrix. *Construction and Building Materials*, *34*, 451-456.

[12] Benmansour, N., Agoudjil, B., Gherabli, A., Kareche, A., & Boudenne, A. (2014). Thermal and mechanical performance of natural mortar reinforced with date palm fibers for use as insulating materials in building. *Energy and Buildings*, *81*, 98-104.

[13] Belhadj, B., Bederina, M., Makhloufi, Z., Dheilly, R. M., Montrelay, N., & Quéneudéc, M. (2016). Contribution to the development of a sand concrete lightened by the addition of barley straws. *Construction and Building Materials*, *113*, 513-522.

[14] Onésippe, C., Passe-Coutrin, N., Toro, F., Delvasto, S., Bilba, K., & Arsène, M. A. (2010). Sugar cane bagasse fibres reinforced cement composites: thermal considerations. *Composites Part A: Applied Science and Manufacturing*, *41*(4), 549-556.

[15] Akinyemi, B. A., & Dai, C. (2020). Development of banana fibers and wood bottom ash modified cement mortars. *Construction and Building Materials*, *241*, 118041.

[16] Swift, D. G., & Smith, R. B. L. (1979). The flexural strength of cement-based composites using low modulus (sisal) fibres. *Composites*, *10*(3), 145-148.

[17] Banthia, N., Moncef, A., Chokri, K. , & Sheng, J. (1995). Uniaxial tensile response of microfibre reinforced cement composites. *Materials and Structures*, *28*(9), 507-517.

[18] Banthia, N., & Sheng, J. (1996). Fracture toughness of micro-fiber reinforced cement concrete. *Cement and concrete composites*, *18*(4), 251-269.

[19] Mihashi, H., & Kohno, Y. (2007). Toughening mechanism of hybrid fiber reinforced cement composites. In *6th International conference on fracture mechanics of concrete and concrete structures*.

[20] Fu, C. Q., Ma, Q. Y., Jin, X. Y., Shah, A. A., & Tian, Y. (2014). Fracture property of steel fiber reinforced concrete at early age. *Computers and Concrete*, *13*(1), 31-47.

[21] Hamdaoui, O., Ibos, L., Mazioud, A., Safi, M., & Limam, O. (2018). Thermophysical characterization of *Posidonia Oceanica* marine fibers intended to be used as an insulation material in Mediterranean buildings. *Construction and Building Materials*, *180*, 68-76.

[22] Gustafsson, S. E. (1991). Transient plane source techniques for thermal conductivity and thermal diffusivity measurements of solid materials. *Review of scientific instruments*, *62*(3), 797-804.

[23] Gustavsson, M., Karawacki, E., & Gustafsson, S. E. (1994). Thermal conductivity, thermal diffusivity, and specific heat of thin samples from transient measurements with hot disk sensors. *Review of Scientific Instruments*, *65*(12), 3856-3859.

[24] Log, T., & Gustafsson, S. E. (1995). Transient plane source (TPS) technique for measuring thermal transport properties of building materials. *Fire and materials*, *19*(1), 43-49.

[25] Krapez, J. C. (2007). Mesure de l'effusivité thermique-Méthodes photothermiques.

[26] EN, N. 12390-3, 2012. *Norme. Essais pour béton durci-Partie*, *3*.

[27] ISO 12135, 2016. Matériaux métalliques – Méthode unifiée d'essai pour la détermination de la ténacité quasi statique.

[28] Pickering, K. L., Efendy, M. A., & Le, T. M. (2016). A review of recent developments in natural fibre composites and their mechanical performance. *Composites Part A: Applied Science and Manufacturing*, *83*, 98-112.

[29] Ibos, L (2012). Métrologie thermique appliquée à la caractérisation thermophysique des composites et au contrôle de structures par thermographie, HDR Université Paris-Est.

[30] Zaroudi, M., Madandoust, R., & Aghaee, K. (2020). Fresh and hardened properties of an eco-friendly fiber reinforced self-consolidated concrete composed of polyolefin fiber and natural zeolite. *Construction and Building Materials*, *241*, 118064.

[31] Nair, S. V. (1990). Crack-wake debonding and toughness in fiber-or whisker-reinforced brittle-matrix composites. *Journal of the American Ceramic Society*, *73*(10), 2839-2847.

[32] Mohr, B. J., Nanko, H., & Kurtis, K. E. (2005). Durability of kraft pulp fiber–cement composites to wet/dry cycling. *Cement and Concrete Composites*, *27*(4), 435-448.

[33] Juarez, C. A., Fajardo, G., Monroy, S., Duran-Herrera, A., Valdez, P., & Magniont, C. (2015). Comparative study between natural and PVA fibers to reduce plastic shrinkage cracking in cement-based composite. *Construction and Building Materials*, *91*, 164-170.

[34] Akhavan, A., Catchmark, J., & Rajabipour, F. (2017). Ductility enhancement of autoclaved cellulose fiber reinforced cement boards manufactured using a laboratory method simulating the Hatschek process. *Construction and Building Materials*, *135*, 251-259.

[35] Bekhiti, M., Trouzine, H., & Rabehi, M. (2019). Influence of waste tire rubber fibers on swelling behavior, unconfined compressive strength and ductility of cement stabilized bentonite clay soil. *Construction and Building Materials*, *208*, 304-313.

[36] Wang, D., Wang, H., Larsson, S., Benzerzour, M., Maherzi, W., & Amar, M. (2020). Effect of basalt fiber inclusion on the mechanical properties and microstructure of cement-solidified kaolinite. *Construction and Building Materials*, *241*, 118085.

[37] Bigg, D. M. (1995). Thermal conductivity of heterophase polymer compositions. In *Thermal and electrical conductivity of polymer materials* (pp.1-30). Springer, Berlin, Heidelberg.

[38] Zhandarov, S., & Mäder, E. (2005). Characterization of fiber/matrix interface strength: applicability of different tests, approaches and parameters. *Composites Science and Technology*, *65*(1), 149-160.

[39] Matthews, F. L., & Rawlings, R. D. (1999). *Composite materials: engineering and science*. CRC press.

[40] Van Hattum, F. W. J., & Bernardo, C. A. (1999). A model to predict the strength of short fiber composites. *Polymer composites*, *20*(4), 524-533.

[41] Beinish, H. Éprouvettes en béton : leurs essais. CERIB, 2000

[42] Neville, A. M. (1995). *Properties of concrete* (Vol. 4). London: Longman.

[43] Yao, W., Jiang, S., Fei, W., & Cai, T. (2017). Correlation between the compressive, tensile strength of old concrete under marine environment and prediction of long-term strength. *Advances in Materials Science and Engineering, 2017, 12.*

[44] Haecker, C. J., Garboczi, E. J., Bullard, J. W., Bohn, R. B., Sun, Z., Shah, S. P., & Voigt, T. (2005). Modeling the linear elastic properties of Portland cement paste. *Cement and Concrete Research*, *35*(10), 1948-1960.

[45] Wambua, P., Ivens, J., & Verpoest, I. (2003). Natural fibres: can they replace glass in fibre reinforced plastics ?. *Composites science and technology*, *63*(9), 1259-1264.

[46] Baley, C. (2014). Fibres naturelles de renfort pour matériaux composites. sl: Techniques de l'ingénieur. *Ref. AM*, *5*, 130.